Draft version July 1, 2010
Preprint typeset using LaTeX style emulateapj v. 11/10/09

INFRARED PROPERTIES OF A COMPLETE SAMPLE OF STAR-FORMING DWARF GALAXIES

Sukbum A. Hong[1], Jessica L. Rosenberg[1]
Department of Physics and Astronomy, George Mason University, Fairfax, VA 22030

Matthew L. N. Ashby[2]
Harvard-Smithsonian Center for Astrophysics, 60 Garden Street, MS 65, Cambridge, MA 02138

and

John J. Salzer[3]
Astronomy Department, Indiana University, Bloomington, IN 47405

Draft version July 1, 2010

ABSTRACT

We present a study of a large, statistically complete sample of star-forming dwarf galaxies using mid-infrared observations from the *Spitzer Space Telescope*. The relationships between metallicity, star formation rate (SFR) and mid-infrared color in these systems show that the galaxies span a wide range of properties. However, the galaxies do show a deficit of 8.0 μm polycyclic aromatic hydrocarbon emission as is apparent from the median 8.0 μm luminosity which is only 0.004 $L^*_{8.0}$ while the median B-band luminosity is 0.05 L^*_B. Despite many of the galaxies being 8.0 μm deficient, there is about a factor of 4 more extremely red galaxies in the [3.6] − [8.0] color than for a sample of normal galaxies with similar optical colors. We show correlations between the [3.6] − [8.0] color and luminosity, metallicity, and to a lesser extent SFRs that were not evident in the original, smaller sample studied previously. The luminosity–metallicity relation has a flatter slope for dwarf galaxies as has been indicated by previous work. We also show a relationship between the 8.0 μm luminosity and the metallicity of the galaxy which is not expected given the competing effects (stellar mass, stellar population age, and the hardness of the radiation field) that influence the 8.0 μm emission. This larger sample plus a well-defined selection function also allows us to compute the 8.0 μm luminosity function and compare it with the one for the local galaxy population. Our results show that below 10^9 $L_\odot$, nearly all the 8.0 μm luminosity density of the local universe arises from dwarf galaxies that exhibit strong Hα emission – i.e., 8.0 μm and Hα selection identify similar galaxy populations despite the deficit of 8.0 μm emission observed in these dwarfs.

Subject headings: galaxies: dwarf – galaxies: fundamental parameters – galaxies: ISM – infrared: galaxies

1. INTRODUCTION

It has become clear that the mid-infrared properties of galaxies are dependent on metallicity (e.g., Engelbracht et al. 2005; Wu et al. 2006; Rosenberg et al. 2006, 2008; Hunt et al. 2006; Madden et al. 2006; O'Halloran et al. 2006). The infrared emission, particularly from polycyclic aromatic hydrocarbon (PAH) grains, is usually driven by the radiation from young stars (Tielens 2008 and references therein). However, the strength of PAH emission is altered and may begin to break down for lower metallicity systems. In the most extreme cases of SBS 0335-052 and I Zw 18, two of the lowest metallicity galaxies known, there is no evidence for PAH emission (Houck et al. 2004; Wu et al. 2007). However these two sources show dramatically different mid-infrared spectral energy distributions (SEDs) that indicate the presence of a cold dust ($T \lesssim 30$K) component in I Zw 18 but not in SBS 0335-052. While metallicity may influence the strength of the PAH features, these galaxies indicate that it is not the key to understanding the mid-infrared slope in the lowest metallicity systems.

shongg@gmu.edu, jrosenb4@gmu.edu
mashby@cfa.harvard.edu
slaz@astro.indiana.edu

The correlation between the PAH emission from galaxies and metallicity has been attributed to the harder radiation field in lower metallicity systems causing the break-down of the PAH molecules (Madden et al. 2006; Wu et al. 2006; O'Halloran et al. 2006) and to the delayed injection of PAH molecules into the interstellar medium due to the youth of the stellar populations (Galliano et al. 2008). Alternatively, the shape of the mid-infrared continuum in galaxies, which is usually attributed to the temperature of the dust and the star formation rate (SFR) in the galaxy, does not seem to be dependent on the metallicity of the system.

In this paper we continue the exploration of the relationship between the mid-infrared properties of galaxies and their metallicity, luminosity, and SFR. We build on the work presented by Rosenberg et al. (2006) for 19 galaxies by discussing the mid-infrared properties of much larger samples of 86 galaxies presented in §3.1. We examine the relationship between colors (§3.2), metallicity (§3.3), and SFR (§3.4) and the properties of galaxies. In §3.5, we use this expanded sample to compute the 8.0 μm luminosity function for the star-forming dwarf galaxies and compare it with that for local galaxies as a whole (Huang et al. 2007). We also use the 8.0 μm luminosity density as a measure of the star formation rate density

(SFRD) and compare it with the value derived from the Hα luminosity density.

Distances throughout this paper are based on $H_0 = 70$ km s^{-1} Mpc^{-1}. All magnitudes discussed in this paper are Vega relative magnitudes.

2. OBSERVATIONS AND DATA REDUCTION

The galaxies in this sample are selected from the KPNO International Spectroscopic Survey (KISS, Salzer et al. 2000), the first fully digital objective prism survey for extragalactic emission-line objects. The galaxies represent a star-forming dwarf ($M_B > -18$) galaxy sub-sample of the KISS galaxies selected by their Hα emission lines. The sample consists of all 60 KISS-selected dwarf galaxies in the 1.3° wide strip centered on δ(B1950)=29°30′ (Salzer et al. 2001) with velocities less than 9000 km s^{-1}. We combine these data with 26 star-forming dwarf galaxies within the Boötes field where no velocity limit has been imposed, 16 of which have velocities greater than 9000 km s^{-1}. The Boötes field is a 8.5 deg^2 region that has been observed both as a part of KISS survey and the NOAO Deep Wide-Field Survey (NDWFS; Jannuzi and Dey 1999). There are 19 galaxies in this field that overlap with Spitzer Shallow Survey area (Eisenhardt et al. 2004). The inclusion of the higher velocity sample increases the number of redder, more luminous sources but it does not change the range of parameter space sampled as we show in the next section. The KISS data for the full sample are presented in Table 1.

Observations of 67 star-forming dwarf galaxies at 3.6, 4.5, 5.8 and 8.0 μm were made in 2006 July using the Infrared Array Camera (IRAC; Fazio et al. 2004) aboard the *Spitzer Space Telescope* (Werner et al. 2004). The basic image processing was reduced using the IRACproc package (Schuster et al. 2006). IRACproc is based on the *Spitzer* Science Center mosaic software MOPEX (Mosaicking and Point-source extraction) and provides enhanced cosmic ray rejection. The resulting mosaiced images are 130″ × 130″ except for KISSR 73 (259″× 259″) and KISSR 1048 (216″×216″) because these systems are more extended. The pixel scale for all images is 0.″86 per pixel.

The measurement of photometry for these galaxies was divided into three processes: point-source subtraction in the 3.6 and 4.5 μm bands, background subtraction, and elliptical isophotal fitting. Stellar crowding was a problem for the galaxy photometry and background estimation in the 3.6 and 4.5 μm bands as seen in the 3.6 μm image shown in Figure 1. The figure shows the aperture in which we measure the galaxy flux (red) and the annulus we use for background subtraction (green). MOPEX/APEX was used to identify and remove point sources from the mosaics, except for sources found to be part of the galaxies in question. Some of the bright point sources in the 3.6 and 4.5 μm bands leave residuals after the subtraction. These residuals and any sources in the galaxy or background area at 5.8 and 8.0 μm were masked before the isophotal fitting was performed in those bands. After the point sources were subtracted and/or masked, the background subtraction and isophotal fitting were done using the ELLIPSE package within

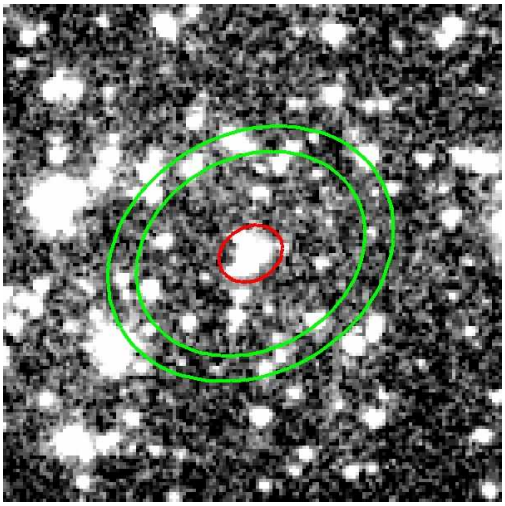

FIG. 1.— 3.6 μm image of KISSR 2378. The red (inner) ellipse shows the aperture in which the galaxy flux was measured. The green (outer) ellipses show the annulus in which the sky background was measured. This figure shows the degree to which stars were a problem for the photometric measurements.

IRAF[1]/STSDAS. The ELLIPSE task was used to fit elliptical isophotes to the galaxy given a fixed center, ellipticity, and position angle. The background was defined as the average intensity in ellipses that are at least 5 pixels beyond the extent of the galaxy (usually within an annulus at a radius of 36–45 pixels except for the four largest systems for which larger annuli were used). The extent of the galaxy was assumed to be the point at which the flux reaches within 1σ of the background level. For two of the galaxies (KISSR148 and KISSR 217) bright point sources introduced a background gradient across the image. For these sources, the IMSURFIT task within IRAF was used to fit a second-order polynomial to the background in order to remove the gradient after the initial background subtraction. After the image was background subtracted, the galaxy flux was measured within the previously determined extent of the galaxy from a second run of the ELLIPSE fitting routine.

The flux errors were assumed to be the combination of the Poisson errors and a systematic error due to the uncertainty in the galaxy extent. The flux error due to the uncertainty in the galaxies' extent was computed to be the change in the measured flux when the galaxy extent was increased or decreased by 1 pixel or by 10%, whichever was larger. The results of the photometry are presented in Table 2. One galaxy, KISSR 85, was not detected in any of the IRAC bands and three additional sources, KISSR 73, KISSR 75, and KISSR 856, were only detected at 3.6 and 4.5 μm. We report upper limits for these sources in Table 2. These limits for the galaxies that were detected at 3.6 μm, were calculated as the number of pixels in the 3.6 μm band aperture multiplied by the standard deviation of the background within the aperture at the appropriate band. We calculated the up-

[1] IRAF is distributed by the National Optical Astronomy Observatories, which is operated by the Association of Universities for Research in Astronomy, Inc. (AURA) under cooperative agreement with the National Science Foundation.

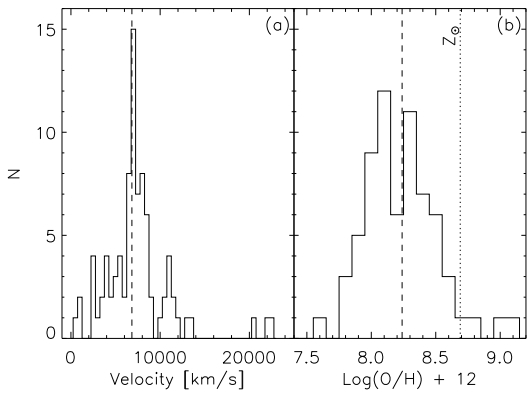

FIG. 2.— Histogram of (a) velocity and (b) metallicity for the star-forming dwarf galaxies. The dashed lines indicate the median values for the sample. The median velocity is 6834 km s^{-1}, the median metallicity is log[O/H]+12 = 8.24 ($0.35Z_\odot$). The dotted line in panel (b) indicates solar metallicity, log[O/H]+12 = 8.69 (Asplund et al. 2009).

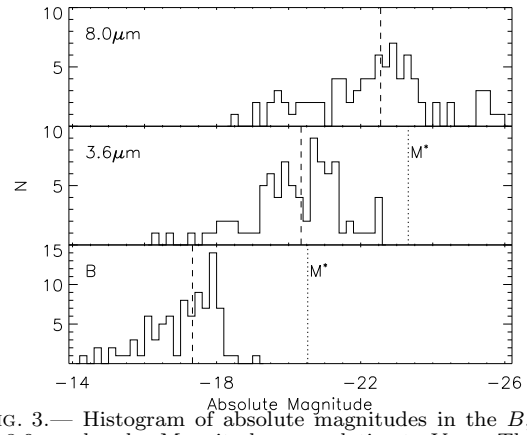

FIG. 3.— Histogram of absolute magnitudes in the B, 3.6 μm and 8.0 μm bands. Magnitudes are relative to Vega. The dashed lines indicate the median magnitudes in each band, $M_B = -17.33$, $M_{3.6} = -20.35$, and $M_{8.0} = -22.55$. Note that these galaxies have been selected to have $M_B > -18$ but ten galaxies are brighter than that limit after being extinction corrected. The dotted lines indicate the characteristic magnitudes, M^*_B and $M^*_{3.6}$. $M^*_{8.0} = -28.46$ so it is off the right edge of the upper panel.

per limit for the galaxy that was not detected in any of the bands as the standard deviation times the number of pixels within a 5 pixel radius aperture.

3. RESULTS

3.1. *Properties of the Sample*

The sample discussed here consists of two sub-samples of KISS galaxies: (1) 26 galaxies located in the Boötes field and (2) 60 galaxies in the KISS 30° strip. Figure 2(a) shows the velocity distribution for the sample. The median for the sample is 6834 km s^{-1}. Most of the galaxies have velocities less than 9000 km s^{-1}, the limit imposed for systems in the 30° strip. In discussing the properties of the galaxies we include 16 galaxies with velocities greater than 9000 km s^{-1} that were observed in the Boötes field. Figure 2(b) shows the metallicity distribution for 67 of the 86 galaxies. The remaining 19 galaxies do not have strong enough lines for the metallicity determination. The median metallicity for galaxies in the sample is log[O/H]+12 = 8.24 ($0.35Z_\odot$) while the lowest metallicity galaxy is only log[O/H]+12 = 7.60 ($0.08Z_\odot$).

The distribution of B, 3.6 μm, and 8.0 μm absolute magnitudes is shown in Figure 3. There are 10 galaxies brighter than $M_{B_0} = -18$ once they are corrected for extinction. The median absolute magnitudes for the sample are $M_{B_0} = -17.33$, $M_{3.6} = -20.35$, and $M_{8.0} = -22.55$, which are indicated with dashed lines in the figure. The B-band luminosities for the sample range from $0.003L^*_B$ to $0.25L^*_B$ (Driver and De Propris 2003) while the range is between $0.002L^*_{3.6}$ and $0.51L^*_{3.6}$ at 3.6 μm (Dai et al. 2009) and between $0.0001L^*_{8.0}$ and $0.09L^*_{8.0}$ at 8.0 μm (Huang et al. 2007). The median 8.0 μm luminosity, $0.004L^*_{8.0}$, is a much smaller fraction of L^* than the median B-band luminosity, $0.05L^*_B$, or 3.6 μm luminosity, $0.06L^*_{3.6}$. The smaller 8.0 μm luminosity with respect to L^* indicates that, as a whole, these systems are deficient in the 8.0 μm emission. This finding is consistent with a drop-off in 8.0 μm emission for low luminosity (Wu et al. 2009) and low-metallicity (Engelbracht et al. 2008) galaxies.

3.2. *Colors of Star-forming Dwarf Galaxies*

Figure 4 shows the relationship between the [3.6] − [8.0] and $B - R$ colors for galaxies in this sample (large blue circles) and for all sources classified as galaxies (black circles) in both the Spitzer Deep, Wide-Field Survey (SDWFS; Ashby et al. 2009; Brown et al. 2007) and the NDWFS (Jannuzi and Dey 1999). The R-band magnitudes are derived from the Sloan Digital Sky Survey (Adelman-McCarthy et al. 2008) r-band magnitudes transformed to Johnson R using the color correction from Fadda et al. (2004). Figure 4 shows that the star-forming dwarf galaxies are significantly bluer in their optical colors than the majority of galaxies because their light is dominated by star formation. The [3.6] − [8.0] color spans the same range covered by late-type galaxy colors in the SDWFS but tend toward the redder end of the galaxy distribution including a few extremely red sources. The star-forming dwarf galaxies with $0 < B-R < 2$ and [3.6] − [8.0] > 2.5 represent almost 40% of the sample, approximately ten times the fraction of SDWFS galaxies in this range and almost four times the fraction of SDWFS galaxies in this range when only galaxies with $0 < B-R < 2$ colors are considered. Expanding this analysis beyond the 19-galaxy sample of Rosenberg et al. (2006, hereafter Paper I) to the 86 galaxies treated here has helped to fill in this color-color plot and improve the statistics, but it has not significantly changed the range of galaxy colors identified except to pick up a few galaxies with redder $B - R$ colors.

Figure 5 presents the $[3.6] - [8.0]_{S.S.}$ color as a function of the 3.6 and stellar subtracted 8.0 μm luminosities. The 8.0 μm magnitude and luminosity has had subtracted using a scale factor of 0.227 of 3.6 μm (Pahre et al. 2004a) as a function of the 3.6 and stellar subtracted 8.0 μm luminosities. The stellar subtracted 8.0 μm flux used here and in some of the figures below as a better measure of the dust emission in this band. The stellar subtracted magnitude is not used in the color-color plots because galaxies with purely stellar colors can not be plotted for comparison since 8.0 μm flux drops to zero. In general, the more luminous galaxies are redder in the $[3.6] - [8.0]_{S.S.}$ color, a trend that was not clear for the 19 galaxies in Paper I. Since the $[3.6] - [8.0]_{S.S.}$ color is

TABLE 1
PROPERTIES OF KISS GALAXIES

KISSR	RA J2000	Dec J2000	V_{hel} (km s^{-1})	M_B	M_{B_0}[a]	$(B-V)_0$[b]	c$_{H\beta}$[c]	log $L_{H\alpha}$ (erg s^{-1})	log[O/H]+12[d]	log(SFR)[e] ($M_\odot$ yr^{-1})
1	12:15:06.9	29:01:10.0	7285	− 17.73	− 17.88	0.50	0.09	40.17	8.53	− 0.87
32	12:21:11.4	29:32:08.7	7855	− 16.61	− 16.76	0.59	0.37	40.24	8.41	− 0.59
40	12:22:23.6	29:26:37.8	7808	− 17.83	− 17.98	0.58	0.40	40.52	8.17	− 0.28
49	12:24:35.2	29:27:32.0	7871	− 17.42	− 17.57	0.58	0.20	40.70	8.24	− 0.25
52	12:25:25.6	29:44:18.2	7981	− 18.00	− 18.15	0.80	1.18	41.08	...	0.86
55	12:26:22.0	29:22:12.5	8067	− 15.92	− 16.07	0.19	0.45	40.14	7.84	− 0.63
57	12:26:39.3	29:37:58.4	6595	− 17.60	− 17.75	0.38	0.64	40.38	8.49	− 0.25
59	12:27:08.7	28:57:22.7	7447	− 17.89	− 18.04	0.65	...	39.93	...	− 1.17
61	12:27:33.4	29:36:06.0	6560	− 15.62	− 15.77	0.52	0.09	39.78	8.10	− 1.26
73	12:31:57.2	29:42:46.3	631	− 14.16	− 14.31	0.34	0.05	38.19	7.91	− 2.87
75	12:32:48.2	29:23:27.3	7899	− 17.26	− 17.41	0.51	0.01	40.12	...	− 0.97
85	12:37:18.5	29:14:54.7	6939	− 15.04	− 15.19	0.11	0.00	39.88	7.60	− 1.22
91	12:39:39.6	29:36:34.2	6989	− 17.12	− 17.27	0.52	0.34	40.48	8.49	− 0.37
105	12:42:53.6	29:17:18.2	6717	− 14.57	− 14.72	0.48	0.01	39.62	7.80	− 1.47
108	12:43:55.3	29:22:11.7	6982	− 17.40	− 17.55	0.36	0.24	40.54	8.23	− 0.38
115	12:46:09.1	28:57:30.6	7019	− 17.82	− 17.97	0.59	0.31	40.46	8.47	− 0.41
119	12:47:24.5	29:12:26.0	6916	− 16.37	− 16.52	0.50	0.74	40.35	...	− 0.20
125	12:48:38.4	29:11:24.9	7037	− 17.76	− 17.91	0.42	0.23	40.36	8.50	− 0.57
133	12:51:06.6	29:11:48.2	6605	− 16.97	− 17.12	0.52	0.48	40.25	8.55	− 0.50
142	12:53:49.2	28:56:33.1	7068	− 17.77	− 17.92	0.87	...	39.79	...	− 1.31
148	12:54:45.3	28:55:29.8	2392	− 15.53	− 15.68	0.14	0.13	39.39	8.31	− 1.62
156	12:57:43.6	29:00:11.9	6833	− 16.95	− 17.10	0.24	0.18	40.03	8.04	− 0.94
170	13:00:31.2	28:57:01.5	6914	− 17.19	− 17.34	0.56	0.81	40.42	8.64	− 0.08
171	13:00:37.2	28:39:50.7	7024	− 16.99	− 17.14	0.72	0.13	39.96	8.81	− 1.05
182	13:02:25.7	28:51:28.9	6645	− 17.63	− 17.78	0.43	0.21	40.51	8.27	− 0.44
187	13:04:16.8	28:51:02.5	7481	− 16.26	− 16.41	0.49	− 0.02	40.08	8.14	− 1.04
191	13:04:38.8	28:58:21.8	7470	− 17.95	− 18.10	0.37	− 0.02	40.15	8.10	− 0.96
192	13:05:06.5	28:38:28.5	5521	− 15.86	− 16.01	0.87	1.11	40.72	...	0.44
193	13:05:12.3	29:14:09.4	6971	− 16.03	− 16.18	0.50	0.85	40.12	8.23	− 0.35
194	13:05:15.5	28:37:35.1	6555	− 17.29	− 17.44	0.49	0.68	40.45	8.33	− 0.15
205	13:07:23.0	29:24:04.0	5211	− 17.10	− 17.25	0.38	0.39	40.24	8.06	− 0.57
207	13:08:04.0	28:59:54.8	7332	− 17.91	− 18.06	0.45	1.99	41.56	8.06	1.93
210	13:08:15.2	29:01:22.4	6131	− 16.58	− 16.73	0.34	...	39.99	...	− 1.12
215	13:08:54.9	29:32:39.5	6764	− 17.84	− 17.99	0.59	1.11	40.82	...	0.54
217	13:09:07.3	28:40:06.6	5577	− 17.59	− 17.74	0.48	0.52	40.44	8.54	− 0.27
236	13:13:35.3	29:07:35.2	5929	− 17.38	− 17.53	0.95	...	39.80	...	− 1.30
238	13:14:37.6	29:19:04.6	6503	− 17.30	− 17.45	0.73	1.44	40.91	...	0.88
245	13:16:28.0	29:25:11.3	4754	− 16.39	− 16.54	0.48	0.49	39.96	8.39	− 0.77
271	13:21:40.8	28:52:59.1	6737	− 17.40	− 17.55	0.67	0.60	40.54	8.31	− 0.12
272	13:21:45.1	29:27:51.6	8912	− 17.23	− 17.38	0.34	0.01	39.99	7.91	− 1.10
278	13:23:37.7	29:17:17.3	4062	− 15.52	− 15.67	0.40	0.03	39.30	8.02	− 1.78
280	13:24:08.7	29:11:04.0	5463	− 15.95	− 16.10	0.52	0.02	39.56	8.06	− 1.53
286	13:26:25.1	29:10:31.5	5161	− 16.53	− 16.68	0.54	0.22	40.73	8.06	− 0.20
299	13:29:56.5	29:46:19.3	7779	− 17.18	− 17.33	0.25	0.28	40.46	8.24	− 0.44
314	13:35:35.6	29:13:00.9	909	− 15.27	− 15.42	0.40	0.31	39.26	8.05	− 1.61
386	13:54:25.8	29:33:00.2	7170	− 17.69	− 17.84	0.63	0.39	40.38	8.36	− 0.43
396	13:57:10.0	29:13:10.1	2317	− 15.03	− 15.18	0.32	...	39.63	7.91	− 1.47
407	13:58:36.1	29:23:20.9	5726	− 17.72	− 17.87	0.47	...	39.93	...	− 1.17
460	14:08:18.8	29:01:01.0	7295	− 17.94	− 18.09	0.84	0.64	40.20	...	− 0.42
505	14:16:55.4	29:29:11.5	3354	− 16.60	− 16.75	0.38	0.54	39.94	7.99	− 0.76
507	14:17:24.7	29:41:11.8	8431	− 17.67	− 17.82	0.73	...	40.08	...	− 1.02
541	14:23:58.3	29:49:33.8	3114	− 16.33	− 16.48	0.48	1.45	40.75	...	0.72
561	14:29:53.6	29:20:10.6	3683	− 15.69	− 15.83	0.29	0.02	39.74	8.08	− 1.35
572	14:46:48.2	29:25:17.1	3794	− 16.12	− 16.27	0.39	− 0.08	39.56	8.34	− 1.60
856	15:46:45.5	29:52:09.3	8385	− 14.48	− 14.63	0.63	...	39.23	...	− 1.87
956	16:02:05.2	29:43:37.8	4410	− 16.66	− 16.81	0.40	0.69	40.15	8.33	− 0.44
1011	16:15:46.5	29:52:53.5	2580	− 15.96	− 16.11	0.52	...	38.98	...	− 2.12
1013	16:16:39.0	29:03:33.0	7540	− 17.44	− 17.59	0.37	0.03	40.14	8.07	− 0.94
1021	16:19:02.6	29:10:22.4	2708	− 15.12	− 15.27	0.27	0.13	39.40	8.03	− 1.60
1048	16:33:47.6	28:59:05.7	1100	− 17.22	− 17.37	0.37	0.02	38.01	8.32	− 3.08
2292	14:25:09.2	35:25:16.0	8659	− 17.80	− 18.31	0.66	0.28	40.39	8.41	− 1.05
2300	14:26:08.9	33:54:19.8	10271	− 16.09	− 16.09	0.50	0.15	40.52	7.89	− 1.10
2302	14:26:17.5	35:21:35.6	8342	− 17.16	− 17.16	0.42	...	40.04	...	− 1.05
2309	14:26:53.6	34:04:14.6	7231	− 17.12	− 17.12	0.43	0.28	40.09	7.98	− 1.52
2316	14:28:14.9	33:30:25.7	10685	− 17.38	− 18.57	0.81	1.09	41.01	9.10	0.12

TABLE 1–Continued

KISSR	RA J2000	Dec J2000	V_{hel} (km s^{-1})	M_B	M_{B_0}[a]	$(B-V)_0$[b]	$c_{H\beta}$[c]	log $L_{H\alpha}$ (erg s^{-1})	log[O/H]+12[d]	log(SFR)[e] ($M_\odot$ yr^{-1})
2318	14:28:24.6	35:10:21.5	22163	− 17.88	− 17.88	0.95	...	41.15	...	0.05
2322	14:29:09.6	32:51:26.8	8574	− 17.84	− 17.84	0.53	0.10	40.24	8.05	− 1.30
2326	14:29:32.7	33:30:40.4	7935	− 17.14	− 17.14	0.51	0.15	40.65	8.00	− 0.96
2338	14:30:27.9	35:32:07.2	11689	− 17.20	− 17.20	0.77	0.19	40.81	8.06	− 0.74
2344	14:31:03.6	35:31:14.8	4166	− 17.75	− 17.75	0.44	0.25	40.12	8.27	− 1.40
2346	14:31:14.4	33:19:13.2	10819	− 16.80	− 16.80	0.67	0.20	40.49	7.84	− 1.15
2349	14:31:20.0	34:38:03.8	4396	− 16.63	− 16.63	0.52	− 0.01	40.48	8.04	− 1.10
2357	14:31:39.2	33:26:32.3	10759	− 17.67	− 17.67	0.58	0.50	40.40	8.37	− 1.05
2359	14:31:49.3	35:28:40.0	22512	− 17.55	− 18.03	0.64	1.35	41.66	8.62	0.32
2368	14:32:18.9	33:02:53.7	10972	− 17.05	− 17.05	0.76	0.19	40.84	8.03	− 0.74
2378	14:33:19.4	32:43:00.0	11171	− 17.79	− 17.79	0.38	0.71	40.85	8.00	0.27
2382	14:34:08.0	34:19:34.5	6813	− 17.81	− 17.81	0.35	0.10	40.03	8.28	− 1.40
2384	14:34:30.1	32:50:46.1	11492	− 17.72	− 17.72	0.45	0.18	40.62	8.24	− 0.35
2398	14:36:33.1	34:58:04.5	9006	− 18.01	− 18.01	0.46	0.19	40.33	8.42	− 1.10
2400	14:37:04.8	33:00:20.4	3797	− 16.54	− 16.54	0.51	0.25	39.58	8.31	− 1.34
2403	14:37:42.6	33:36:26.7	12047	− 16.24	− 16.24	0.36	0.36	40.38	8.36	− 1.05
2406	14:38:27.8	35:08:59.1	8641	− 17.89	− 17.89	0.49	0.19	40.38	8.35	− 1.05
2407	14:38:29.3	33:20:07.5	20385	− 17.51	− 17.51	0.53	0.94	41.25	...	0.85
2412	14:38:51.5	34:29:52.8	9845	− 16.29	− 16.29	0.62	0.15	40.45	7.95	− 0.54
2413	14:38:59.5	34:22:51.8	13110	− 17.69	− 19.04	0.86	0.61	40.77	9.03	0.12
2415	14:39:17.6	34:22:21.2	13265	− 16.88	− 17.96	0.76	1.14	41.07	8.71	0.81

[a] B-band absolute magnitude corrected for internal extinction using the ad hoc method from (Melbourne and Salzer 2002).
[b] $B-V$ color corrected for Galactic absorption.
[c] Decimal reddening coefficient.
[f] A measure of metallicity. For detail of the calculation see Melbourne and Salzer (2002) and Salzer et al. (2005).
[e] SFR calculated from the Hα luminosity using the prescription of Kennicutt (1998).

TABLE 2
Spitzer IRAC Photometry

KISSR	$R_{3.6}$ (arcsec)[a]	Ellipticity[b]	[3.6]	$\sigma_{3.6}$	[4.5]	$\sigma_{4.5}$	[5.8]	$\sigma_{5.8}$	[8.0]	$\sigma_{8.0}$
1	15.0	0.0	14.14	0.07	14.16	0.11	13.55	0.21	11.99	0.08
32	6.9	0.2	14.85	0.11	14.82	0.15	13.50	0.21	11.77	0.07
40	13.6	0.2	14.25	0.08	14.31	0.12	13.46	0.20	12.33	0.09
49	9.0	0.3	14.71	0.10	14.72	0.14	13.88	0.24	12.34	0.10
52	15.6	0.4	12.88	0.05	12.98	0.07	11.58	0.09	9.76	0.03
55	5.4	0.2	16.93	0.29	16.66	0.34	16.84	0.71	15.30	0.37
57	17.6	0.6	14.26	0.08	14.14	0.11	13.24	0.18	12.23	0.09
59	28.9	0.7	12.54	0.03	12.65	0.05	11.07	0.07	9.36	0.01
61	5.7	0.3	16.48	0.23	16.38	0.29	15.67	0.48	14.93	0.30
73	38.6	0.4	13.16	0.04	13.10	0.08	> 10.96	···	> 10.34	···
75	12.6	0.0	15.34	0.06	15.41	0.08	> 13.76	···	> 13.17	···
85	4.3	0.0	> 18.75	···	> 17.79	···	> 15.75	···	> 15.04	···
91	9.6	0.2	14.03	0.08	14.03	0.11	12.50	0.14	10.81	0.05
105	4.3	0.0	17.64	0.39	17.32	0.46	16.59	0.74	15.27	0.41
108	12.3	0.6	14.75	0.10	14.71	0.14	13.95	0.25	12.37	0.09
115	10.5	0.0	13.79	0.07	13.79	0.09	13.13	0.18	11.56	0.06
119	8.9	0.3	15.54	0.15	15.67	0.22	15.26	0.42	13.65	0.18
125	10.1	0.3	13.82	0.07	13.83	0.10	12.51	0.14	10.88	0.05
133	15.8	0.6	13.94	0.07	14.01	0.11	12.84	0.16	11.20	0.05
142	21.2	0.4	13.03	0.05	13.21	0.08	12.45	0.13	11.66	0.06
148	18.4	0.4	14.17	0.07	14.06	0.09	13.15	0.18	12.03	0.06
156	12.5	0.0	14.99	0.12	15.02	0.16	14.65	0.34	13.28	0.14
170	25.8	0.7	13.86	0.07	14.05	0.11	12.83	0.15	11.26	0.06
171	11.8	0.4	14.34	0.09	14.31	0.12	13.51	0.21	12.83	0.06
182	10.3	0.0	14.27	0.08	14.37	0.12	13.48	0.21	12.06	0.08
187	10.0	0.5	15.83	0.18	15.73	0.23	15.10	0.44	13.57	0.15
191	12.2	0.0	14.11	0.08	14.09	0.11	13.46	0.20	12.15	0.09
192	18.8	0.7	14.77	0.10	14.71	0.14	13.75	0.23	12.23	0.09
193	6.0	0.3	16.23	0.20	16.24	0.28	15.72	0.50	14.63	0.25
194	8.2	0.3	14.28	0.08	14.31	0.12	13.54	0.20	12.19	0.09
205	10.2	0.0	14.46	0.09	14.40	0.12	14.06	0.26	12.81	0.11
207	25.0	0.8	14.12	0.08	14.26	0.12	13.53	0.21	12.02	0.07
210	10.2	0.1	15.15	0.12	15.09	0.16	14.48	0.31	12.90	0.12
215	13.1	0.4	13.21	0.05	13.16	0.06	12.08	0.11	10.40	0.04
217	14.4	0.0	13.65	0.06	13.59	0.07	12.53	0.13	11.12	0.06
236	20.4	0.4	12.13	0.03	12.21	0.05	11.00	0.07	9.23	0.02
238	11.3	0.3	13.68	0.07	13.73	0.09	13.47	0.20	12.71	0.11
245	8.7	0.0	14.48	0.09	14.54	0.14	13.32	0.19	11.83	0.07
271	9.5	0.0	14.04	0.08	13.93	0.10	13.35	0.19	11.96	0.08
272	10.8	0.1	14.81	0.11	14.68	0.15	14.52	0.29	13.22	0.14
278	9.2	0.2	15.39	0.14	15.33	0.19	15.38	0.46	14.33	0.25
280	9.8	0.4	15.47	0.15	15.53	0.21	15.77	0.55	14.69	0.26
286	7.6	0.0	14.35	0.09	14.24	0.12	13.25	0.19	11.78	0.08
299	5.9	0.0	15.05	0.12	14.94	0.16	14.14	0.27	12.59	0.10
314	32.6	0.4	12.46	0.03	12.80	0.05	12.97	0.12	11.39	0.04
386	15.5	0.6	14.04	0.08	14.07	0.11	13.36	0.20	11.92	0.08
396	9.2	0.0	14.93	0.11	14.78	0.14	14.50	0.32	14.02	0.20
407	15.1	0.2	13.81	0.06	13.81	0.09	13.19	0.18	11.82	0.08
460	22.0	0.5	12.53	0.04	12.59	0.06	11.28	0.08	9.58	0.03
505	14.2	0.4	14.00	0.07	13.94	0.10	13.55	0.21	12.81	0.10
507	12.6	0.3	14.18	0.08	14.19	0.11	13.66	0.22	12.14	0.09
541	14.5	0.4	13.70	0.06	13.66	0.09	13.15	0.18	12.39	0.08
561	12.4	0.4	15.44	0.14	15.43	0.19	15.41	0.42	14.57	0.25
572	16.7	0.6	14.43	0.09	14.37	0.12	13.46	0.20	12.28	0.09
856	5.2	0.0	15.33	0.14	15.23	0.18	> 15.39	···	> 14.80	···
956	13.5	0.5	14.11	0.08	14.11	0.11	13.55	0.21	12.17	0.09
1011	23.8	0.5	13.66	0.06	13.86	0.10	13.58	0.21	12.23	0.09
1013	11.8	0.6	15.21	0.13	15.15	0.17	14.84	0.36	13.56	0.15
1021	9.0	0.1	15.09	0.12	15.04	0.16	14.76	0.36	13.25	0.15
1048	62.3	0.3	10.82	0.01	10.59	0.01	9.59	0.02	8.49	0.01
2292	12.0	0.1	14.31	0.07	14.29	0.09	13.53	0.17	12.15	0.07
2300	10.0	0.3	16.59	0.19	16.32	0.24	15.96	0.51	14.40	0.19
2302	14.0	0.3	16.05	0.15	16.03	0.21	15.81	0.47	15.04	0.25
2309	12.0	0.2	15.40	0.11	15.43	0.16	14.92	0.32	14.18	0.17
2316	14.0	0.1	14.15	0.06	14.09	0.08	12.61	0.11	10.61	0.03

TABLE 2–Continued

KISSR	$R_{3.6}$ (arcsec)[a]	Ellipticity[b]	[3.6]	$\sigma_{3.6}$	[4.5]	$\sigma_{4.5}$	[5.8]	$\sigma_{5.8}$	[8.0]	$\sigma_{8.0}$
2318	14.0	0.3	15.50	0.11	15.31	0.15	14.68	0.28	12.27	0.07
2322	20.0	0.2	14.76	0.08	14.68	0.11	14.31	0.24	12.93	0.10
2326	14.0	0.2	15.39	0.11	15.33	0.15	14.56	0.27	13.18	0.11
2338	14.0	0.2	15.82	0.13	15.49	0.16	14.60	0.27	12.89	0.09
2344	70.0	0.7	12.66	0.03	12.53	0.04	11.56	0.07	10.80	0.04
2346	12.0	0.1	15.88	0.14	15.80	0.19	15.25	0.37	13.67	0.14
2349	20.0	0.3	14.39	0.07	14.10	0.09	12.94	0.13	11.47	0.05
2357	20.0	0.6	15.19	0.10	15.01	0.13	14.89	0.31	13.42	0.12
2359	12.0	0.1	16.14	0.16	15.96	0.20	15.69	0.45	13.03	0.10
2368	14.0	0.4	15.89	0.14	15.45	0.16	14.57	0.27	12.75	0.09
2378	8.5	0.2	15.67	0.15	15.42	0.18	15.07	0.40	14.18	0.21
2382	20.0	0.4	14.17	0.06	14.16	0.09	13.47	0.16	12.07	0.06
2384	6.9	0.2	15.43	0.14	15.28	0.18	14.60	0.32	13.11	0.13
2398	30.0	0.4	14.27	0.07	14.17	0.09	13.39	0.16	11.98	0.06
2400	24.0	0.7	13.96	0.07	14.08	0.11	13.40	0.19	12.40	0.09
2403	14.0	0.3	16.96	0.23	16.78	0.29	15.81	0.47	14.88	0.23
2406	20.0	0.1	14.25	0.06	14.26	0.09	13.40	0.16	11.93	0.06
2407	8.6	0.6	16.03	0.19	15.88	0.24	15.58	0.47	14.72	0.28
2412	5.6	0.0	16.28	0.21	16.21	0.27	16.17	0.59	14.33	0.24
2413	8.2	0.0	13.99	0.08	13.93	0.10	12.63	0.14	10.52	0.04
2415	5.9	0.0	14.87	0.11	14.72	0.14	13.26	0.19	11.15	0.05

[a] The semimajor axis of the aperture in which the flux was measured.
[b] The ellipticity of the fit aperture.

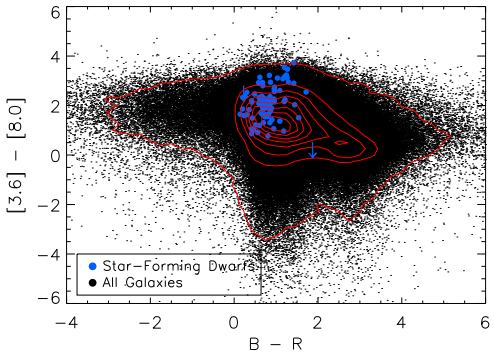

FIG. 4.— [3.6] − [8.0] vs. $B - R$ colors for the star-forming dwarf galaxies (blue circles) and for galaxies in both the SDWFS (Ashby et al. 2009; Brown et al. 2007) and NDWFS (Jannuzi and Dey 1999) with $m_{3.6} < 20$ (black circles). Two galaxies have upper limits at the [3.6] − [8.0] are indicated by arrows. Contours indicate the density of the black circles.

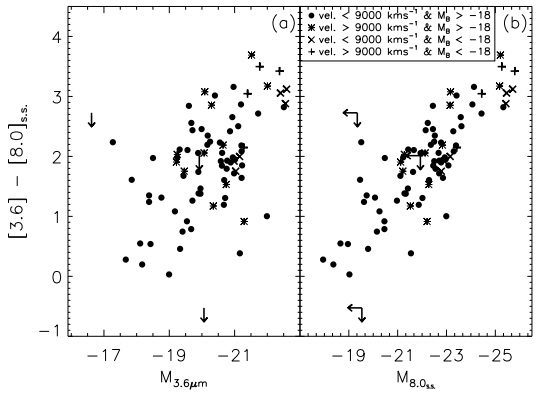

FIG. 5.— $[3.6] - [8.0]_{S.S.}$ color as a function of the 3.6 and stellar subtracted 8.0 μm absolute magnitude. The filled circles indicate galaxies with velocities smaller than 9000 km s^{-1} and with absolute B magnitudes dimmer than −18. The asterisks indicate galaxies with velocities larger than 9000 km s^{-1} and with absolute B magnitudes dimmer than −18. The crosses indicate galaxies with velocities smaller than 9000 km s^{-1} and with absolute B magnitudes brighter than −18. The plus signs indicate galaxies with velocities larger than 9000 km s^{-1} and with absolute B magnitudes brighter than −18. Several of the galaxies have upper limits only at 8.0 μm and are indicated by arrows in both color and, in the $M_{8.0}$ plot, absolute magnitude.

a good proxy for the mass-normalized dust content (8.0 μm probes PAH plus hot dust continuum while 3.6 μm traces the stellar mass), redder galaxies being more luminous indicates that the dust emission per unit stellar mass increases both as stellar mass (3.6 μm luminosity) and total dust emission from the galaxy (8.0 μm luminosity) increase. The mass normalized dust content of a galaxy appears to be better correlated with the total dust content of the system (correlation coefficient = −0.79) than it is with the total stellar mass (correlation coefficient = −0.45). This difference in correlation seems to indicate that the process that regulates the average dust emission in these galaxies – either the delayed injection of dust due to the youth of the stellar population or the destruction of dust in the hard stellar radiation field – has a significant impact on the total dust luminosity of the galaxy but is not strongly tied to the bulk stellar mass.

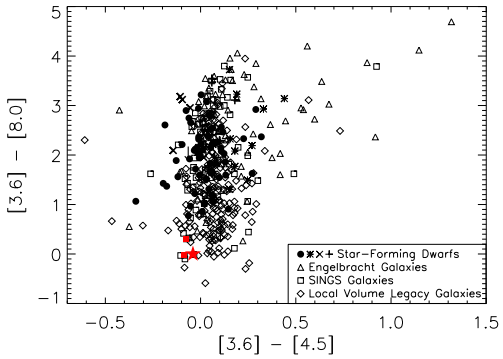

FIG. 6.— [3.6] − [8.0] vs. [3.6] − [4.5] color–color diagram. The galaxies in our sample are shown by the same symbols as in Figure 5. Star-forming galaxies from Engelbracht et al. (2005) are shown as open triangles, SINGS (Kennicutt et al. 2003) are shown as open squares, and LVL galaxies (Dale et al. 2009) are shown as open diamonds. The red star indicates the theoretical colors of M0 III stars (Pahre et al. 2004b) for reference. In addition, the red filled squares indicate the observed colors of elliptical galaxies with the dust-free fitting SED model in SINGS.

Figure 6 shows the [3.6] − [8.0] versus [3.6] − [4.5] color–color plot for the galaxies in this sample, starburst galaxies from Engelbracht et al. (2005), galaxies from *Spitzer* Infrared Nearby Galaxies Survey (SINGS; Kennicutt et al. 2003), and galaxies from the *Spitzer* Local Volume Legacy (LVL; Dale et al. 2009). The SINGS samples cover a wide range of morphologies, metallicities, SFRs, and infrared-to-optical ratios in normal galaxies (Kennicutt et al. 2003). The LVL sample includes all galaxies within 11 Mpc down to a magnitude limit of $m_B = 15$. This complete sampling of the local volume includes the full range of galaxy types from ellipticals to spirals and irregulars. The [3.6] − [8.0] color of the KISS galaxies spans the blue end of the range covered by the LVL galaxies. Our sample does not have galaxies as red in the [3.6] − [8.0] color as those in LVL because we do not include early-type systems. There is little correlation between the [3.6] − [8.0] and [3.6] − [4.5] colors with the exception of the reddest galaxies ([3.6] − [4.5] > 0.4) which are all red in the [3.6] − [8.0] color ([3.6] − [8.0] > 1.5). Most of the galaxies fall within a relatively small range of the [3.6] − [4.5] color around the colors of a theoretical M0 III star (Pahre et al. 2004b) and the SINGS elliptical galaxies NGC 0584 and NGC 1404 (Dale et al. 2007). We use NGC 0584 and 1404 as fiducial dust-free ellipticals because their spectra show no evidence for dust emission in the mid-infrared[2]. The galaxies with the reddest [3.6] − [4.5] color ([3.6] − [4.5] > 0.7) are primarily luminous systems from Engelbracht et al. (2005). The lack of dwarf galaxies with these red colors indicates that hot dust does not make a significant contribution to the 4.5 μm emission in these galaxies. The [3.6] − [4.5] colors are bluer than the theoretical M0 III stellar color and the fidical dust-free elliptical galaxies for a few of the galaxies possibly indicating emission in the 3.6 μm band from the 3.3 μm PAH feature.

3.3. *Effect of Metallicity on the Properties of Star-forming Dwarf Galaxies*

[2] See http://web.ipac.caltech.edu/staff/jarrett/rac/carlibration/galaxies.html.

The luminosity–metallicity relationship is fundamental to galaxies and their evolution, connecting the star formation history in galaxies to the increase in metal abundance. Tremonti et al. (2004) used the SDSS to extend this relationship to a stellar mass–metallicity relationship and found that the lower mass systems are more prone to metal loss, probably through galaxy winds that preferentially remove metals from the lower potential systems.

Figure 7 shows the relationship between metallicity and M_{B_0}, $M_{3.6}$ and $M_{8.0_{S.S.}}$. Most of the galaxies in our sample are sub-solar ($[\log(\mathrm{O/H}) + 12]_\odot = 8.69$). The luminosity-metallicity relationships for galaxies fainter than $M_B = -18$ in our sample are determined from a linear least-squares fit to the data points giving the relations:

$$\log(\mathrm{O/H}) + 12 = -0.15(\pm0.03)M_{B_0} + 5.73(\pm0.50)$$
$$\log(\mathrm{O/H}) + 12 = -0.13(\pm0.02)M_{3.6} + 5.62(\pm0.43)$$
$$\log(\mathrm{O/H}) + 12 = -0.09(\pm0.02)M_{8.0_{S.S.}} + 6.24(\pm0.34)$$

giving an rms scatter around the fits of 0.20 at B-band, 0.18 at 3.6 μm, and 0.18 at 8.0 μm. The slope of these relations is consistent with the slope determined from 19 data points in Paper I, although we now get a slightly shallower slope at B-band and 3.6 μm and a slightly steeper slope at 8.0 μm which brings all of the values in all three bands closer together. For comparison with our B-band data, we show the linear least-squares fit to the full KISS sample (including $M_B < -18$, Melbourne and Salzer 2002). This B-band slope is significantly shallower than that determined for the full KISS sample (Melbourne and Salzer 2002, -0.24) and for Blue Compact Dwarf Galaxies (Zhao et al. 2010, -0.24). This flattening at the low-luminosity end is consistent with other values obtained for dwarf galaxies (van Zee and Haynes 2006; Shi et al. 2005; Lee et al. 2004; Richer and McCall 1995; Skillman et al. 1989) and has been previously noted by Melbourne and Salzer (2002). The flattening of the slope of this relation at lower luminosity implies that the dwarf galaxies have a relatively larger metallicity than the more luminous systems. This difference could be driven by a floor on the metallicity or differences in the astrophysical processes (e.g., outflows versus closed-box enrichment) that govern this relationship.

The 3.6 μm luminosity–metallicity relationship is expected to be tighter than the B-band relationship because it is less influenced by extinction and it is a better measure of the stellar mass of the system (as noted in the previous section, it does not appear to be strongly influenced by PAH emission at 3.3 μm). However, we find only a modest decrease in the scatter between B-band and 3.6 μm. Even more surprising, the scatter in the 8.0 μm relationship is the same as for the 3.6 μm relationship. We would expect the dependence of the 8.0 μm luminosity on the combination of the PAH and dust continuum emission which are influenced by the SFR, the radiation field, and possibly the age of the stellar population to increase the scatter.

Figure 8 shows the relationship between the mid-infrared colors of galaxies and metallicity for galaxies in our sample, star-forming dwarf galaxies from Engelbracht et al. (2005), and galaxies from SINGS (Kennicutt et al. 2003). The mass-normalized dust content of galaxies in Figure 8(a) is correlated with the metallicity, although there is a lot of scatter in the relationship. Like the color–luminosity relationship, this correlation was not evident with the smaller sample in Paper I. The linear least-squares fit on the log scale to the relationship is

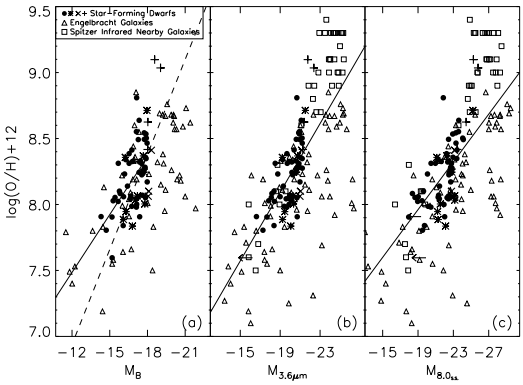

FIG. 7.— Metallicity as a function of absolute magnitude in the B, 3.6, and $8.0_{S.S.}$ μm bands. The galaxies in our sample are shown by the same symbols as in Figure 5. SINGS galaxies (Kennicutt et al. 2003) are shown as open squares and star-forming galaxies from Engelbracht et al. (2005) are shown as open triangles. The solid lines indicate the linear least-squares fits to the data in this sample with $M_{B_0} > -18$. The dashed line in panel (a) shows the slope of the metallicity–luminosity relation from Melbourne and Salzer (2002) for the full sample of KISS galaxies.

$$[3.6] - [8.0]_{S.S.} = 1.41(\pm0.39) \times [\log(\mathrm{O/H})+12] - 9.70(\pm3.23)$$

with an rms scatter around the fit of 0.67 and correlation coefficient 0.43. The large scatter in this relationship indicates that variations in color are being driven by more than the effect of metallicity on the dust emission from the galaxies. The average [3.6] − [4.5] color is 0.1 for the KISS dwarfs. This color is slightly redder than expected for a stellar SED (see Figure 6) indicating that the color of some of the galaxies is being influenced by hot dust in the 4.5 μm band. As indicated by Figure 6, there are galaxies with substantially redder colors than the average indicating hot dust emission at 4.5 μm, than the average – primarily luminous systems in the Engelbracht et al. (2005) sample.

3.4. *Effect of Star Formation Rate on the Properties of Star-forming Dwarf Galaxies*

The galaxies in this sample have been selected because they have Hα emission detected in the KISS objective-prism survey. In addition, we have made a luminosity cut to select dwarf systems. While these two cuts limit the properties of the sample, they still make up a fairly diverse group ranging from strongly star-forming blue compact dwarf galaxies to more diffuse star-forming irregular galaxies. Most of the galaxies exhibit SFRs ranging between 0.001 and 10 $M_\odot$ yr^{-1}. For three sources, the SFRs are even lower than this limit and KISSR 207 has a huge SFR at 85 $M_\odot$ yr^{-1}, although it does not quite make our luminosity cutoff with $M_{B_0} = -18.06$.

As expected, the SFR in these galaxies is correlated with the blue luminosity as shown in Figure 9(a). The SINGS galaxies are included in the plot for comparison over a wider range in luminosity and SFR. We also show the relationship between the SFR and $M_{3.6}$ and $\mathrm{M}_{8.0_{S.S.}}$.

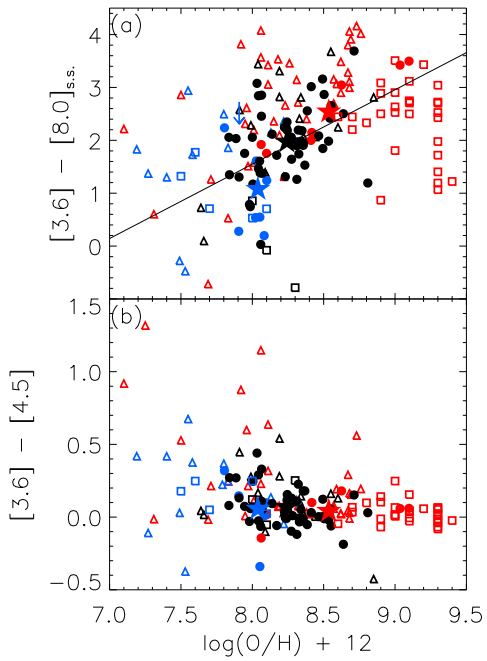

FIG. 8.— [3.6] − [8.0]$_{S.S.}$ and [3.6] − [4.5] color as a function of metallicity. The galaxies in our sample are shown as filled circles. SINGS galaxies are shown as open squares and star-forming galaxies from Engelbracht et al. (2005) are shown as open triangles. We divide our sample into three groups based on their magnitude at B band. Blue points are low-luminosity sources ($M_B > -16$), black points are moderate-luminosity sources ($-18 < M_B < -16$), and red points are high-luminosity sources ($M_B < -18$). Filled stars indicate the average value for each of these magnitude groups. The solid line in panel (a) indicates the linear least squares fit to the data with $M_{B_0} > -18$.

With only two exceptions, all of the high SFR galaxies have high, or unknown metallicities. However, the middle and low-metallicity sources are well mixed at the moderate and low SFRs. The relationships between the SFR and luminosity for our sample are

$$\log(\mathrm{SFR}) = -0.39(\pm0.08)M_{B_0} - 7.37(\pm1.42)$$
$$\log(\mathrm{SFR}) = -0.32(\pm0.07)M_{3.6} - 7.21(\pm1.36)$$
$$\log(\mathrm{SFR}) = -0.18(\pm0.05)M_{8.0_{S.S.}} - 4.81(\pm1.07)$$

with an rms scatter of 0.66 at B-band, 0.66 at 3.6 μm, and 0.65 at 8.0 μm. There are two outliers in this plot – KISSR 207 is a low metallicity galaxy (log(O/H) + 12 = 8.06) with the highest SFR, 85 $M_\odot$ yr^{-1} in the sample, although its luminosity, $M_{B_0} = 18.06$, is just above our nominal limit. KISSR 1048 is a moderate metallicity source (log(O/H) + 12 = 8.32) with the lowest SFR in the sample, but it is moderately bright in all bands ($M_{B_0} = -17.4$).

Figure 10 shows the relationship between mid-infrared colors and both the SFR and the specific star formation rate (SSFR; SFR/$M_{stellar}$). The stellar mass used to calculate the SSFR was derived from the $B-V$ color and the B-band luminosity (Bell and de Jong 2001). There is a correlation between the [3.6] − [8.0] color and the SFR driven mostly by the highest metallicity sources in the sample. The linear least squares fit on the log scale to these data is given by:

$$[3.6] - [8.0]_{S.S.} = 0.27(\pm0.13) \times \log(\mathrm{SFR}) + 2.02(\pm0.13)$$

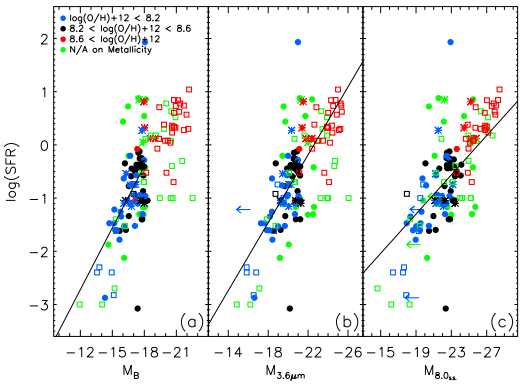

FIG. 9.— SFR, computed from the galaxies Hα luminosity, as a function of absolute magnitude in the B, 3.6, and 8.0$_{S.S.}$ μm bands. The galaxies in our sample are shown as filled circles (velocity < 9000 km s^{-1}) and asterisks (velocity > 9000 km s^{-1}). SINGS galaxies are shown as open squares. We divide our sample into three groups based on their metallicity. Blue points are low-metallicity systems (log(O/H)+12 < 8.2), black points are moderate-metallicity (8.2 < log(O/H)+12 < 8.6), and red points are high-metallicity (log(O/H)+12 > 8.6). Green points are galaxies for which metallicity information is not available. The lines show linear least squares fits to the galaxies with $M_{B_0} > -18$.

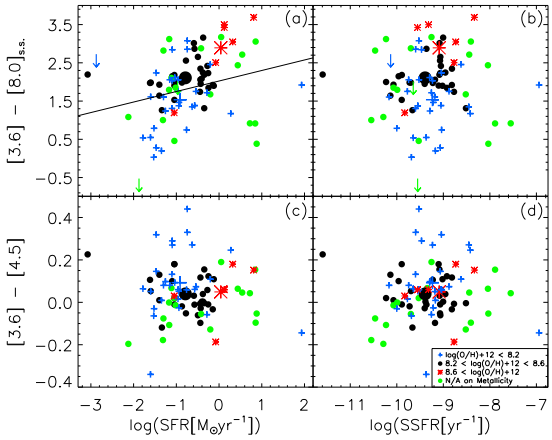

FIG. 10.— [3.6] − [8.0]$_{S.S.}$ and [3.6] − [4.5] as a function of the SFR and the SSFR. The sample is divided into three groups based on their metallicity. Blue plus signs are low-metallicity systems (log(O/H)+12 < 8.2), black circles are moderate-metallicity (8.2 < log(O/H)+12 < 8.6), and red asterisks are high-metallicity (log(O/H)+12 > 8.6). Green circles are galaxies for which metallicity information is not available. Large plus signs, asterisks, and black filled circles indicate the average value for each of these metallicity groups. The solid line in panel (a) indicates the linear least-squares fit to the data with $M_{B_0} > -18$. KISSR 207, the highest SFR source is brighter than $M_{B_0} = -18$ and is not included in the fit.

which has an rms scatter of 0.75 and correlation coefficient 0.25. The major outliers in this plot include the highest SFR source KISSR 207 (blue cross on the far right) which is more luminous than our nominal cutoff of $M_B = -18$, KISSR 1048, the lowest SFR source in the sample, and KISSR 238, 541, 2407 which have high SFRs and bluer [3.6] − [8.0]$_{S.S.}$ colors. The relationship for the 19 galaxies in Paper I had an rms scatter of 0.56 and correlation coefficient 0.66, so the increase in sample size has increased the number of outliers and, overall, decreased the correlation.

The relationship between [3.6] − [8.0]$_{S.S.}$ color and SSFR shows virtually no correlation (correlation coeffi-

cient = 0.02). This lack of a correlation is somewhat surprising given the correlation between 8.0 μm luminosity and SFR since this relation is the same one normalized by stellar mass since 3.6 μm luminosity is a good probe of stellar mass. The SSFR in Figure 10 is computed using stellar mass calculated with the Bell and de Jong (2001) calibration for optical colors, but the plot is almost identical if the stellar mass is computed using the 3.6 μm luminosity with the calibration of Zhu et al. (2010). SFR is correlated with both 3.6 and 8.0 μm luminosities as shown in Figures 9(b) and (c) so the lack of correlation between $[3.6] - [8.0]_{S.S.}$ color and SSFR in Figure 10 indicates that on a global scale in these galaxies, the higher 8.0 μm luminosity in higher SFR galaxies is more strongly driven by the mass of the galaxy than by the star formation processes (i.e., more massive galaxies are also the more luminous and higher SFR galaxies in general). This result is also reflection of the significant contribution made by the dust continuum emission, which is not a function of the SFR, to the 8.0 μm luminosity in these galaxies. Because this continuum contribution is significant the $[3.6] - [8.0]_{S.S.}$ color is not correlated with SSFR.

3.5. *8.0 μm Luminosity Function*

The 8.0 μm luminosity function of star-forming dwarf galaxies is a measure of the contribution of these systems to the total 8.0 μm luminosity density in the local universe. We compute the luminosity function based on the 57 galaxies in the sample with velocities between 1000 and 9000 km s^{-1}. We exclude the lowest velocity, and hence most nearby sources because they are detected in such a small effective volume that they are strongly influenced by the local galaxy density and they contribute disproportionately to the luminosity function. We also exclude galaxies with $v_{hel} > 9000$ km s^{-1} because they are above our velocity cut in the 30° strip. The calculation was carried out using the $1/V_{max}$ method (Schmidt 1968), where V_{max} is the volume corresponding to the maximum redshift at which the galaxy's Hα emission line could have been detected by the survey. In addition, we compute a luminosity function based on an estimate of the stellar subtracted 8.0 μm emission which represents the contribution of PAHs and the hot dust continuum to the 8.0 μm band. The stellar subtracted 8.0 μm luminosity is the 8.0 μm luminosity minus the 3.6 μm luminosity scaled down by a factor of 0.227 (Pahre et al. 2004a), the stellar contribution from an M0 III star.

In Figure 11, we plot the 8.0 μm luminosity function for these galaxies and for an 8.0 μm - selected sample in the Boötes field (Huang et al. 2007). The luminosity function error bars for the star-forming dwarf galaxies are based on Poisson statistics (Gehrels 1986) which correspond to 1σ Gaussian errors. Because we restrict our sample to the faint end of the luminosity function, we do not have a good constraint on the luminosity function's shape. However, the dwarf galaxy luminosity follows the shape of the full sample within the errors and the luminosity density (3.1×10^6 $L_\odot$ Mpc^{-3}) is comparable to the Huang et al. (2007) luminosity (2.9×10^6 $L_\odot$ Mpc^{-3}) density below 10^9 $L_\odot$ indicating that 8.0 μm and Hα selection recover the same 8.0 μm luminosity density, when their respective selection limits are taken into account.

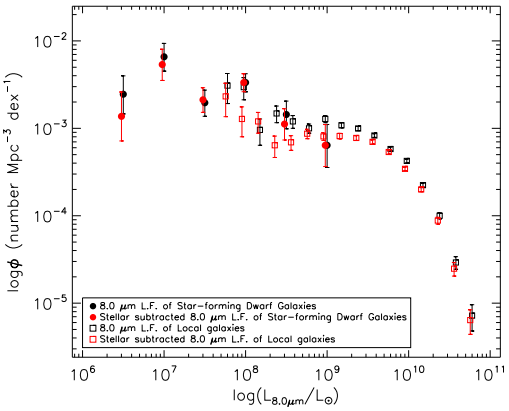

FIG. 11.— Luminosity function for our sources (filled circles) and for a complete 8.0 μm selected sample in the Boötes field (Huang et al. 2007, open squares). The black points are the full 8.0 μm luminosity function while the red points show the stellar continuum subtracted values. These two sets of points have been artificially offset (stellar subtracted numbers to left) so that they are both visible since in most cases they lie on top of one another.

The fraction of the total 8.0 μm luminosity density that comes from star-forming dwarf galaxies is derived from the integration of the luminosity function. We find the luminosity density to be 3.1×10^6 $L_\odot$ Mpc^{-3} or 2.9×10^6 $L_\odot$ Mpc^{-3} if we use the stellar continuum subtracted values. This number is in contrast to the luminosity density derived for all galaxies in the Boötes field of 2.8×10^7 $L_\odot$ Mpc^{-3} or 2.3×10^7 $L_\odot$ Mpc^{-3} if stellar continuum subtracted values are considered (Huang et al. 2007). The relationship between these SFRD (SFRD) values indicates that star-forming dwarf galaxies contribute ~12% of the 8.0 μm luminosity in the local universe which is comparable to the fraction of the Hα luminosity density that they contribute.

4. SUMMARY

We have presented *Spitzer*/IRAC observations of 86 star-forming dwarf galaxies selected from the KISS optical objective prism survey. We build on the previous study of a much smaller number (19) of these galaxies (Paper I) to increase our understanding of the infrared emission from low-luminosity, low-metallicity galaxies. In addition we make use of the statistically complete nature of this sample to examine the luminosity function and luminosity density of these galaxies at 8.0 μm.

Overall the dust emission in these galaxies is clearly affected by both the metallicity and the SFR. We see much better correlations with the 8.0 μm luminosity than we do with the [3.6] − [8.0] color, especially in the case of the SFR. Nevertheless, there are correlations between the [3.6] − [8.0] color and both luminosity and metallicity (and to a much lesser extent SFR) than was evident from the sample of 19 galaxies. More specifically we find the following.

- The median 8.0 μm luminosity in the sample is $0.004L^*$ while the median value at B-band and 3.6 μm is $0.06L^*$. This lower luminosity with respect to L^* at 8.0 μm implies that there is a deficit of hot dust and PAH emission in these galaxies with respect to the majority of galaxies.

- As we found previously with the smaller sample, star-forming dwarf galaxies have much bluer than average optical colors and span a wide range of infrared colors. In [3.6] − [8.0], the galaxies range from very red objects to the colors of early type galaxies. The fraction of very red star-forming dwarf galaxies is almost 4 times higher than it is for SDWFS galaxies with similar optical colors.

- The larger sample investigated in this paper indicates that the [3.6] − [8.0] color is correlated with luminosity, metallicity, and to a much lesser extent SFR. These relationships were not evident with the smaller sample presented in Paper I.

- The luminosity–metallicity relationship for star-forming dwarf galaxies has a shallower slope than what is found for the full KISS sample, consistent with the low-luminosity slope of the SDSS relationship. The change in the slope of this relation with luminosity may indicate either a floor in the metallicity of galaxies or differences in the astrophysical processes (e.g., outflows versus closed-box enrichment) that govern this relationship.

- The relationship between luminosity, particularly at 8.0 μm, and SFR indicates that the 8.0 μm luminosity is another probe of the SFR in galaxies despite the fact that the [3.6] − [8.0] color shows a much stronger correlation with metallicity than with SFR. While there is a small correlation between the [3.6] − [8.0] color and the SFR, there is no apparent correlation when we consider the relationship between color and specific SFR.

- The consistency between the 8.0 μm luminosity function and density derived indicates that below 10^9 $L_\odot$, nearly all the 8.0 μm luminosity density comes from dwarf galaxies that exhibit strong Hα emission – i.e., 8.0 μm and Hα selection identify similar galaxy populations. These galaxies span a similar range of SFRs and have similar space densities.

- The 8.0 μm luminosity is, on average, a good indicator of SFR in these dwarf systems as measured by the comparison of the SFRD computed from the 8.0 μm and Hα emission. This is despite the deficit of hot dust and PAH emission in the star-forming dwarf galaxies (see the first point), the poor correlation between the [3.6] − [8.0] color and the SFR, and the large spread in the SFR versus 8.0 μm luminosity relationship.

This work is based in part on observations made with the *Spitzer Space Telescope*, which is operated by the Jet Propulsion Laboratory, California Institute of Technology under NASA contract 1407. Support for this work was provided by NASA through an IRAC GTO award issued by JPL/Caltech under contract 1256790. J. J. S. gratefully acknowledges support for the KISS project from the NSF through grants AST 95-53020, AST 00-71114, and AST 03-07766. This work also made of data products provided by the SDSS. The SDSS is managed by the Astrophysical Research Consortium for the Participating Institutions. The Participating Institutions are the American Museum of Natural History, Astrophysical Institute Potsdam, University of Basel, University of Cambridge, Case Western Reserve University, University of Chicago, Drexel University, Fermilab, the Institute for Advanced Study, the Japan Participation Group, Johns Hopkins University, the Joint Institute for Nuclear Astrophysics, the Kavli Institute for Particle Astrophysics and Cosmology, the Korean Scientist Group, the Chinese Academy of Sciences (LAMOST), Los Alamos National Laboratory, the Max-Planck-Institute for Astronomy (MPIA), the Max-Planck-Institute for Astrophysics (MPA), New Mexico State University, Ohio State University, University of Pittsburgh, University of Portsmouth, Princeton University, the United States Naval Observatory, and the University of Washington.

REFERENCES

Adelman-McCarthy, J. K. et al. 2008, *ApJS* **175**, 297
Ashby, M. L. N. et al. 2009, *ApJ* **701**, 428
Asplund, M., Grevesse, N., Sauval, A. J., and Scott, P.: 2009, *ARA&A* **47**, 481
Bell, E. F. and de Jong, R. S.: 2001, *ApJ* **550**, 212
Brown, M. J. I., Dey, A., Jannuzi, B. T., Brand, K., Benson, A. J., Brodwin, M., Croton, D. J., & Eisenhardt, P. R.: 2007, *ApJ* **654**, 858
Dai, X. et al. 2009, *ApJ* **697**, 506
Dale, D. A. et al. 2007, *ApJ* **655**, 863
Dale, D. A. et al. 2009, *ApJ* **703**, 517
Driver, S. and De Propris, R.: 2003, *Ap&SS* **285**, 175
Eisenhardt, P. R. et al. 2004, *ApJS* **154**, 48
Engelbracht, C. W., Gordon, K. D., Rieke, G. H., Werner, M. W., Dale, D. A., and Latter, W. B.: 2005, *ApJ* **628**, L29
Engelbracht, C. W., Rieke, G. H., Gordon, K. D., Smith, J., Werner, M. W., Moustakas, J., Willmer, C. N. A., and Vanzi, L.: 2008, *ApJ* **678**, 804
Fadda, D., Jannuzi, B. T., Ford, A., and Storrie-Lombardi, L. J.: 2004, *AJ* **128**, 1
Fazio, G. G. 2004, *ApJS* **154**, 10
Galliano, F., Dwek, E., and Chanial, P.: 2008, *ApJ* **672**, 214
Gehrels, N.: 1986, *ApJ* **303**, 336
Houck, J. R. et al. 2004, *ApJS* **154**, 211
Huang, J. et al. 2007, *ApJ* **664**, 840
Hunt, L. K., Thuan, T. X., Sauvage, M., and Izotov, Y. I.: 2006, *ApJ* **653**, 222
Jannuzi, B. T. and Dey, A.: 1999, in *ASP Conf. Ser. 191: Photometric Redshifts and the Detection of High Redshift Galaxies*, pp 111–+
Kennicutt, R. C.: 1998, *ApJ* **498**, 541
Kennicutt, Jr., R. C. et al. 2003, *PASP* **115**, 928
Lee, J. C., Salzer, J. J., and Melbourne, J.: 2004, *ApJ* **616**, 752
Madden, S. C., Galliano, F., Jones, A. P., and Sauvage, M.: 2006, *A&A* **446**, 877
Melbourne, J. and Salzer, J. J.: 2002, *AJ* **123**, 2302
O'Halloran, B., Satyapal, S., and Dudik, R. P.: 2006, *ApJ* **641**, 795
Pahre, M. A., Ashby, M. L. N., Fazio, G. G., and Willner, S. P.: 2004a, *ApJS* **154**, 235
Pahre, M. A., Ashby, M. L. N., Fazio, G. G., and Willner, S. P.: 2004b, *ApJS* **154**, 229
Richer, M. G. and McCall, M. L.: 1995, *ApJ* **445**, 642
Rosenberg, J. L., Ashby, M. L. N., Salzer, J. J., and Huang, J.-S.: 2006, *ApJ* **636**, 742
Rosenberg, J. L., Wu, Y., Le Floc'h, E., Charmandaris, V., Ashby, M. L. N., Houck, J. R., Salzer, J. J., and Willner, S. P.: 2008, *ApJ* **674**, 814

Salzer, J. J. et al. 2000, *AJ* **120**, 80
Salzer, J. J. et al. 2001, *AJ* **121**, 66
Salzer, J. J., Lee, J. C., Melbourne, J., Hinz, J. L., Alonso-Herrero, A., and Jangren, A.: 2005, *ApJ* **624**, 661
Schmidt, M.: 1968, *ApJ* **151**, 393
Schuster, M. T., Marengo, M., and Patten, B. M.: 2006, in *Proc. SPIE* **6270**, 65
Shi, F., Kong, X., Li, C., and Cheng, F. Z.: 2005, *A&A* **437**, 849
Skillman, E. D., Kennicutt, R. C., and Hodge, P. W.: 1989, *ApJ* **347**, 875
Tielens, A. G. G. M.: 2008, *ARA&A* **46**, 289
Tremonti, C. A. et al. 2004, *ApJ* **613**, 898
van Zee, L. and Haynes, M. P.: 2006, *ApJ* **636**, 214
Werner, M. W. et al. 2004, *ApJS* **154**, 1
Wu, R., Hogg, D. W., and Moustakas, J.: 2009, arXiv:0907.1783
Wu, Y., Charmandaris, V., Hao, L., Brandl, B. R., Bernard-Salas, J., Spoon, H. W. W., and Houck, J. R.: 2006, *ApJ* **639**, 157
Wu, Y. et al. 2007, *ApJ* **662**, 952
Zhao, Y., Gao, Y., and Gu, Q.: 2010, *ApJ* **710**, 663
Zhu, Y., Wu, H., Li, H., and Cao, C.: 2010, *Research in Astronomy and Astrophysics* **10**, 329